

Entanglement Hamiltonians for Free Fermion Chains with Defects

Gavin Rockwood

Department of Physics and Astronomy, Rutgers University, 136 Frelinghuysen Rd,
Piscataway, NJ 08854, US

Abstract. We study the half system entanglement Hamiltonians of the ground state of free fermion critical transverse field Ising model with periodic boundary conditions in the presence of defects. In general, we see that these defects introduce non-local terms into the entanglement Hamiltonian with the largest being couplings across the defect that decay with distance. It is also shown that the entanglement Hamiltonian does know of the defect even if the defect is outside of the subsystem. We also discuss what happens when defects are on the boundaries of the subsystem, and in particular, we investigate the behavior as the bond leading into the subsystem is cut. Finally, we examine the non-local behavior of the antiperiodic defect and duality defect, both of which introduce zero modes.

Contents

1	Introduction	2
2	Free Fermion Techniques	4
3	Single Centered Defect	6
3.1	Comparison with \bar{A}	8
3.2	Off Center Defect	9
4	Periodic with Antipodal Defects	11
5	Defects on Subsystem Boundary	12
5.1	One End	12
5.2	Both Ends	14
6	Defects With Zero Modes	16
6.1	Antiperiodic Defect	16
6.2	Duality Defect	17
7	Conclusion and Future Work	18
	Bibliography	19

1. Introduction

Entanglement entropy is a generally useful and easy to compute quantity to measure entanglement in quantum systems. The first step to calculating the entanglement entropy in a bipartite system is to calculate the reduced density matrix

$$\rho_A = \text{Tr}_{\bar{A}} |\psi\rangle \langle \psi| \quad (1.0.1)$$

where $|\psi\rangle$ is a pure state. The entanglement entropy is then given by the Von-Neumann entropy of the reduced density matrix

$$S_A = -\text{Tr} \rho_A \log \rho_A. \quad (1.0.2)$$

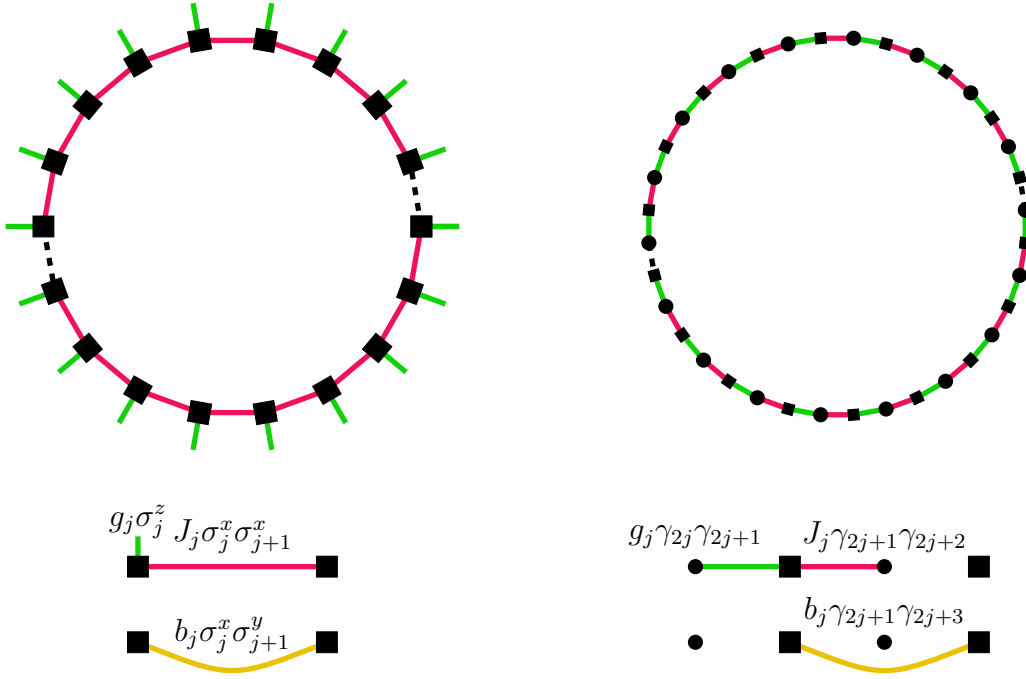


Figure 1: The general geometry before (on left) and after (on right) the Jordan Wigner transform. Post JW transform, we end up with a Majorana hopping model where the duality defect (in gold) leads to a term that skips a Majorana site.

The entanglement entropy, however, distills all the information of ρ_A down into a single number and doesn't capture all there is to know about $|\psi\rangle$. Another object of interest is the entanglement Hamiltonian \mathcal{K}_A , defined as

$$\rho_A = \frac{1}{Z} e^{-\mathcal{K}_A}, \quad (1.0.3)$$

This is also called the modular Hamiltonian. In this form, ρ_A takes on the appearance of a thermal ensemble of the modular Hamiltonian, and we can begin exploring the properties of \mathcal{K}_A . The most natural first question is about $\text{Spec } \mathcal{K}_A$, the entanglement spectrum, which is directly related to the Schmidt spectrum by $\epsilon_i + \epsilon_0 = -\log \lambda_i^2$, where $\epsilon_0 = -\log Z$.[‡] In this paper, we are interested in the transverse field Ising model given by equation 1.0.4. In general, we will be setting $J_i = g_i = 1$ with exception of one or two bond defects, J_i^* .

$$H = -\frac{1}{2} \sum_{i \in \mathbb{Z}_N} (J_i \sigma_i^x \sigma_{i+1}^x + g_i \sigma_i^z) \quad (1.0.4)$$

The motivation for this paper comes out of figure 2, where we have calculated the entanglement entropy and entanglement spectra for spin chains where the subsystem A is half the system and contained at the center of A is an energy defect (Single case) and

[‡] It is also common to see the entanglement Hamiltonian written as $\rho_A = e^{-\mathcal{K}_A}$, in which case $\epsilon_i = -\log \lambda_i^2$. In this paper we pull out the vacuum energy and write it as the $1/Z$ factor equation 1.0.3.

where \bar{A} also contains a defect opposite the one in A (Antipodal case). As the system size N grows, the lattice effects become less important, and the entanglement entropies of all these configurations converge. The entanglement entropy is effectively ignorant of the defect; however, the defect has a impact on the entanglement spectra. This means that \mathcal{K}_A must also have knowledge of these defects and the goal of this paper is to figure out how \mathcal{K}_A depends on these defects using high precision free fermion techniques.

This is not the first work to discuss high precision calculations of entanglement Hamiltonians using free fermion methods. For small critical systems, see [1, 2]; for two disjoint intervals, see [3]; for non-critical spin chains, see [4]; for global quenches, see [5]. Also see [6] for a more general review on entanglement Hamiltonians.

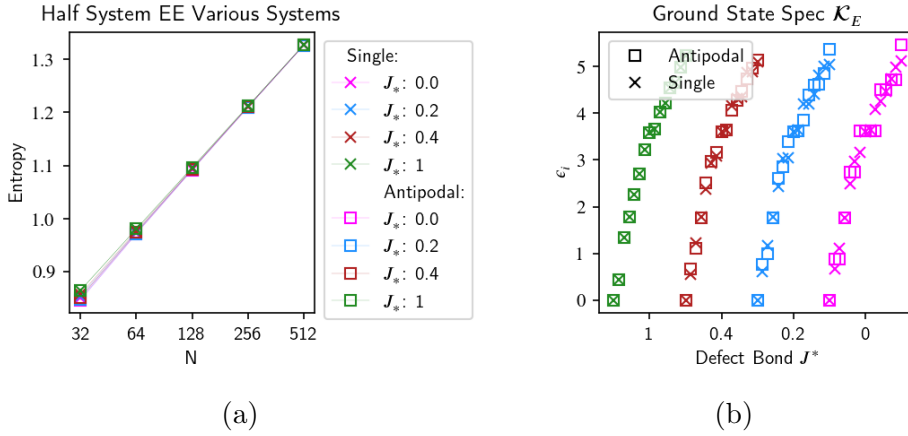


Figure 2: a) Entanglement entropy for various single and antipodal energy defects as a function of system size N . b) The entanglement spectra for systems of size $N = 8129$ for various single and antipodal defects. The colors correspond to the defect strength, and the offset is just for visual clarity and is a function of the eigenvalue index.

2. Free Fermion Techniques

The entanglement Hamiltonian of a free complex fermion system can be written as $\mathcal{K}_A = \sum_{i,j \in A} (K_A)_{ij} c_i^\dagger c_j$ where the matrix K_A is given by the equation

$$K_A = -\log [G_A^{-1} - \mathbb{1}] , \quad (2.0.1)$$

where G_A is the restriction of two correlation matrix $G_{ij} = \langle c_i^\dagger c_j \rangle$ to indices in A [7]. Because we will be going between the Majorana fermions and complex fermions according to

$$c_i^\dagger = \gamma_{2i} + i\gamma_{2i+1}, \quad c_i = \gamma_{2i} - i\gamma_{2i+1}, \quad (2.0.2)$$

we will denote the correlation matrix for the complex fermions as G_A^C and G_A^M for the Majorana fermions coming from $G_{mn}^M = \langle \gamma_m \gamma_n \rangle$. This is important to keep track of as the spectrum of G^M is twice that of G^C .

Following [8] to obtain G_A^M , we start with a Hamiltonian for $2N$ Majorana fermions written as $\mathcal{H} = \frac{1}{2} \sum_{mn} H_{mn} \gamma_m \gamma_n$, where H is an antisymmetric matrix with purely imaginary entries and is thus Hermitian. We then perform real Schur decomposition on $A = -2iH$ and obtain $A = UBU^\dagger$. Because we are doing real Schur decomposition, B will be a matrix of the form

$$B = \bigoplus_{i=0}^{N-1} \begin{pmatrix} 0 & -\epsilon_i \\ \epsilon_i & 0 \end{pmatrix}. \quad (2.0.3)$$

The two point correlation matrix is then given by $G^M = \mathbb{1} + i\Gamma_A$ where $\Gamma_A = U\Gamma_B U^\dagger$ with

$$\Gamma_B = \bigoplus_{i=0}^{N-1} \begin{pmatrix} 0 & -1 \\ 1 & 0 \end{pmatrix}. \quad (2.0.4)$$

The reduced correlation matrix is then given by the restriction of G to some sub-region A . To obtain the entanglement Hamiltonian matrix K , we calculate $K = -\log \left[2 \left(G_A^M \right)^{-1} - \mathbb{1} \right]$. Because $\frac{1}{2} G_A^M$ has eigenvalues that are increasingly close to 0 and 1, evaluating this equation requires decimal precision on the order of the system size. This was also observed in [1, 2] where they looked at subsystems of size $L = 40$. In this paper, using the mpmath package [9], we push this to total system of size $N = 512$. Most of these calculations were done with a decimal precision (dps) of $1.5N$ and for some, $2N$. It should also be noted that when looking at K , we will be keeping it in the Majorana basis such that $\mathcal{K}_A = \sum_{m,n \in A} (K_A)_{mn} \gamma_m \gamma_n$. In this basis, K_A will be purely imaginary and of dimension $2L$ for a subsystem of L complex fermions. **For all of our plots of Majorana K and its elements, it will be implied that we are plotting $\text{im } K$.** Results for a no defect critical, periodic TFI chain are shown in figure 3 as a baseline for comparison. The important take away from figure 3 is that the entanglement Hamiltonian, while not technically local (as K_A is dense), is dominated by local interactions. These Hamiltonians are in agreement with the analytic results from [1].

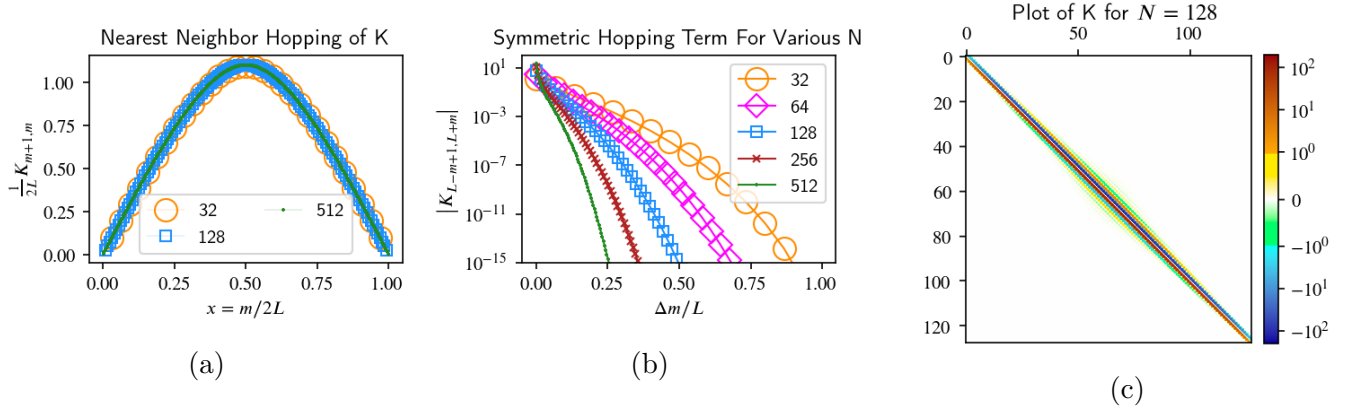


Figure 3: All the figures are looking at elements of K for no defect. a) Plot of Nearest neighbor couplings of K . b) Plot of the symmetric hopping terms / anti-diagonal entries of K_A (for example coupling the first and last sites of the subsystem). These terms are the largest non-local terms in the entanglement Hamiltonian and will become prominent when defects are introduced. c) Plot of the entries of K . The scale is symmetric log where the linear threshold is ± 1 .

3. Single Centered Defect

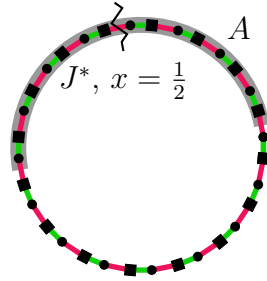


Figure 4: Diagram for the setup for the defect in A .

We begin by looking at the simplest case, a single energy defect in the center subsystem $A = \{0, \dots, N/2 - 1\}$ as shown in figure 4. Before getting to the entanglement Hamiltonian, we can first look at the fermionic log negativity across the defect[10, 11], show in figure 5. For J^* non-zero, we see that the negativity grows like $\log N$, but when $J^* = 0$, the negativity is asymptotically flat and non-zero. This means there is always some amount of entanglement generated by interactions through \bar{A} and thus some amount of terms that couple across the defect. However, we should also expect these couplings to have different system size dependence than the normal nearest neighbor interactions (which should grow linearly with N), in order to give a relatively system size independent negativity for $J^* = 0$.

With this in mind, we begin with figure 6. In 6abd we see the impact of the defect on the nearest neighbor interactions. Most notably, the effect is fairly localized, spanning

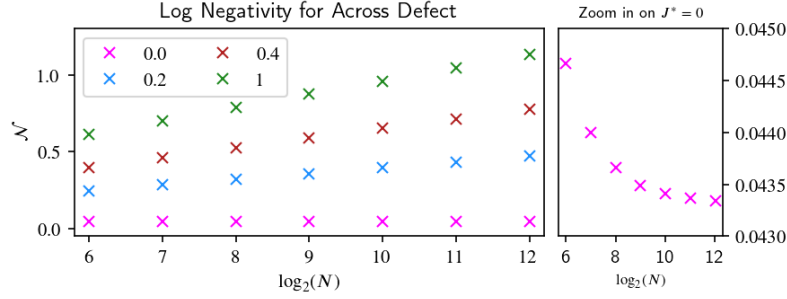


Figure 5: Fermionic log negativity between the left and right halves of A separated by the defect. Here the subsystem is of size $L = N/2$ with the defect at its center. Note that for $J^* = 0$, the negativity is asymptotically flat and non-zero. This means that there is always some amount of entanglement between A_L and A_R through \bar{A} .

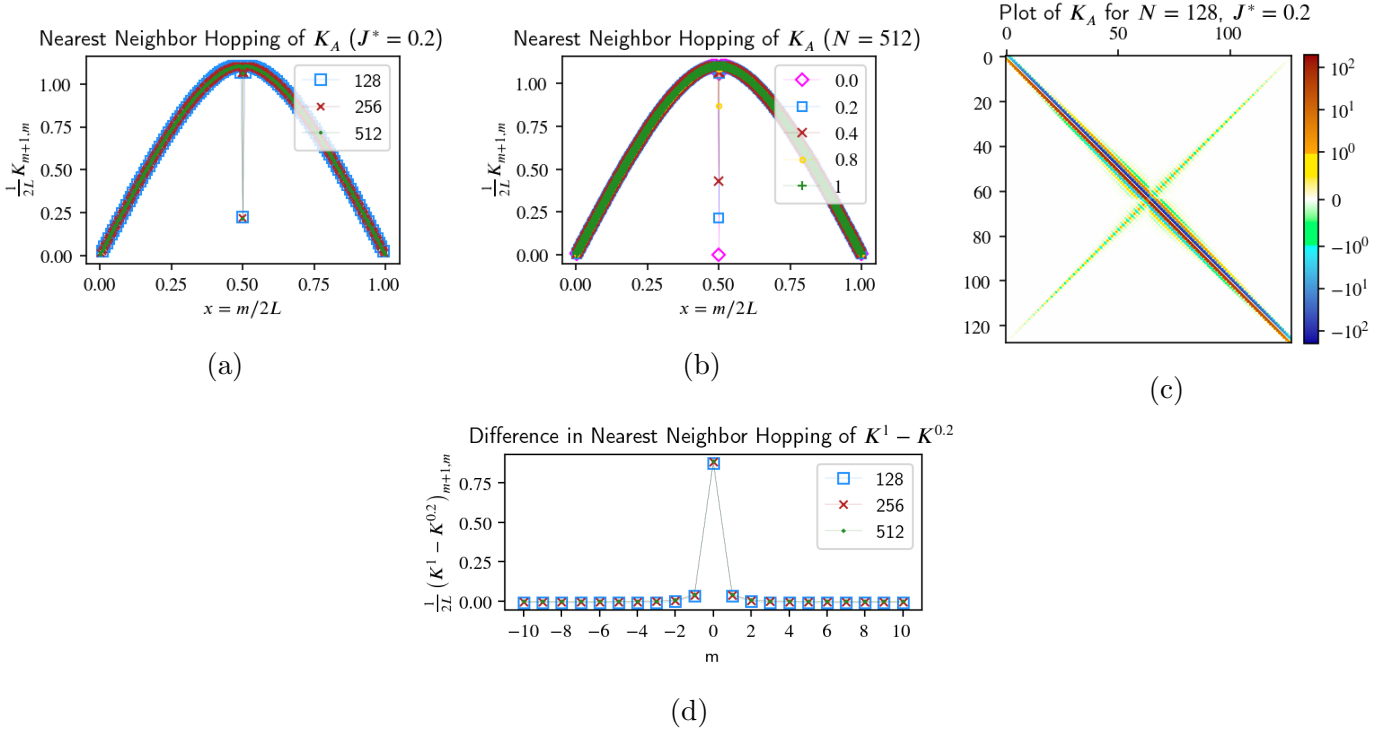


Figure 6: a) Plot of nearest neighbor interactions for various system sizes for $J^* = 0.2$. b) Plot of nearest neighbor interactions for various defects for $N = 512$. c) The full coupling matrix K for $N = 128$ and $J^* = 0.2$. The scale is symmetric log where the linear threshold is ± 1 . Note the prominent anti-diagonal entries, which are symmetric hopping terms across the defect. d) A plot of the nearest neighbor interactions for $K^1 - K^{0.2}$, where K^1 is the K matrix for no defect. The x axis is the lattice distance from the defect ($m = 0$). Note that regardless of system size, the impact of the defect on the nearest neighbor interactions is only a couple lattice sites.

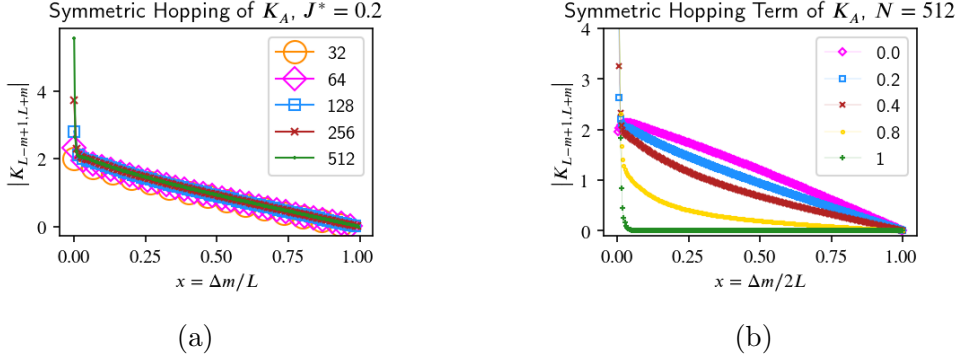


Figure 7: Plots of the symmetric hopping term $K_{L-m+1, L+m}$. Note that in these plots, the defect term itself is left out ($m = 0$). a) Symmetric hopping term for $J^* = 0.2$ for various system sizes. Note that after a few lattice sites away from the defect, the magnitude of these terms does not depend on the system size (there is no factor of $1/2L$ rescaling K , unlike in plots of the nearest neighbor terms). b) Plots of the symmetric hopping terms for various defect strengths. These terms grow with as $J^* \rightarrow 0$. It is also important to note that for both of these plots, we are looking at $|K_{L-m+1, L+m}|$ and there is actually an alternating minus sign.

only a few lattice sites with this width (in terms of m) being system size independent. However, in 6c, we see that there is a prominent anti-diagonal feature which is the symmetric hopping terms across the defect (shown in detail in figure 7). These terms are system size independent in terms of $x = m/L$ after a few lattice sites away from the defect. While these system size independent terms are small, they are responsible for the non-vanishing entanglement negativity seen in figure 5. It is also worth noting that in the K matrix, the defect bond is non-zero when $J^* = 0$; however, it is $\mathcal{O}(1)$ and is relatively system size independent, following the same behavior as the rest of the symmetric hopping terms. This system size independent behavior was also seen in the intersubsystem coupling from [3] for disconnected subsystems.

3.1. Comparison with \bar{A}

We know that the entanglement spectrum of ρ_A and $\rho_{\bar{A}}$ must be the same, and thus the defect should have some impact on $K_{\bar{A}}$. We see (figure 8) the impact on the nearest neighbor interactions is negligible. For small system sizes, there is a slight drop in nearest neighbor coupling strength on the bonds opposite the defect; however, this decreases with system size. The symmetric hopping terms however are the biggest difference (figure 9). Unlike K_A , these hoppings in $K_{\bar{A}}$ show little variation in shape away from $J^* = 1$. Also, away from the defect (x approaching 1), the symmetric hopping terms of K_A and $K_{\bar{A}}$ are in close agreement.

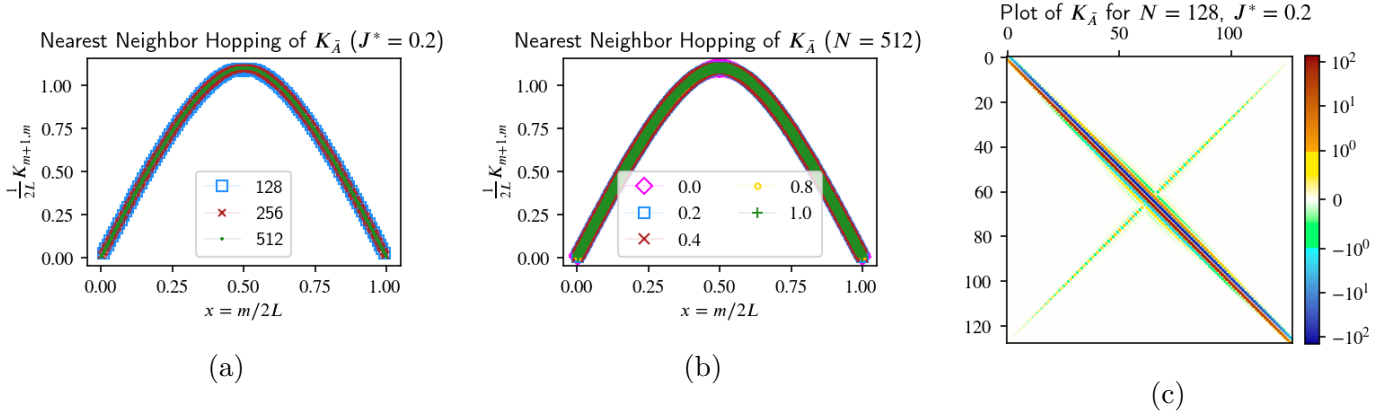


Figure 8: This is the same as figure 6, except now we are looking at \bar{A} . Note that while \bar{A} contains no defects, we get an entanglement Hamiltonian that is highly non-local. $K_{\bar{A}}$ is sensitive to the defect.

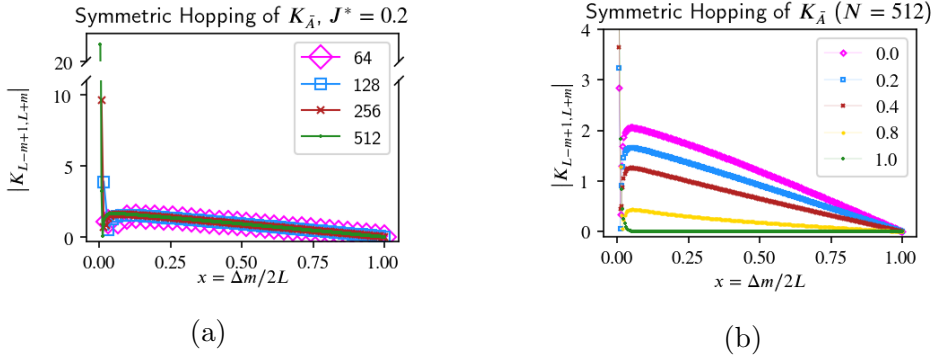


Figure 9: Plots of the symmetric hopping term $K_{L-m+1,L+m}$. a) Various system sizes. b) Various defect strengths.

3.2. Off Center Defect

So far we have looked at K_A and $K_{\bar{A}}$ for a centered energy defect. Now, we move it off center. We expect that, like the centered defect, the impact of the defect should be fairly localized around the defect, which is what we see in figures 10a,b. The important feature of note here is that the cross defect couplings have deformed.

We wrap up this discussion by looking at $K_{\bar{A}}$ for the off center defect. In figure 12 we see that the the non-local couplings across the defect are weaker and no longer symmetric. They have also migrated towards the boundary on the side of the defect.

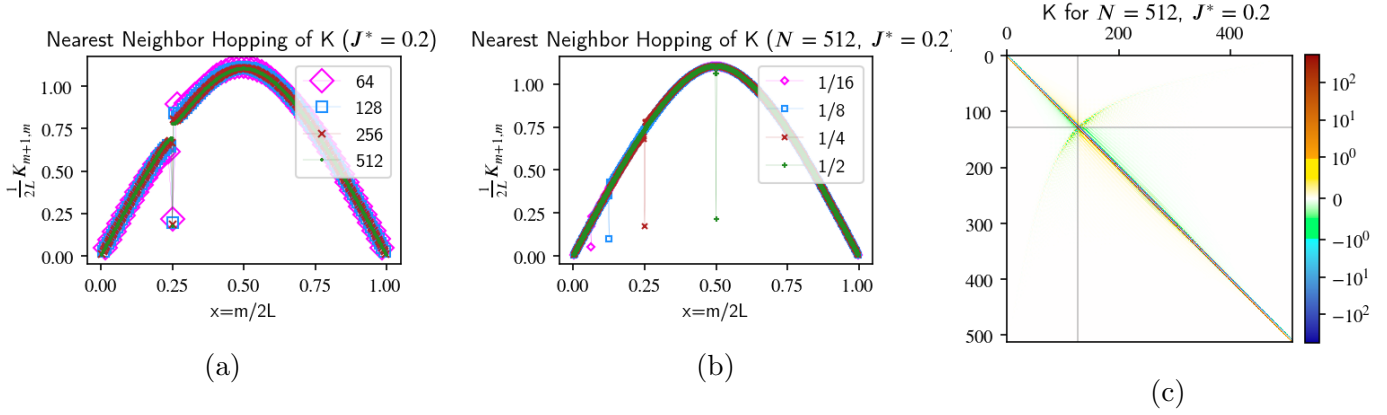


Figure 10: a) Plot of the nearest neighbor hopping terms of K_A for multiple system sizes. b) Plot of the nearest neighbor hopping terms for multiple defect locations. c) Symmetric log plot of K_A . A closeup of the cross defect couplings can be seen in figure 11.

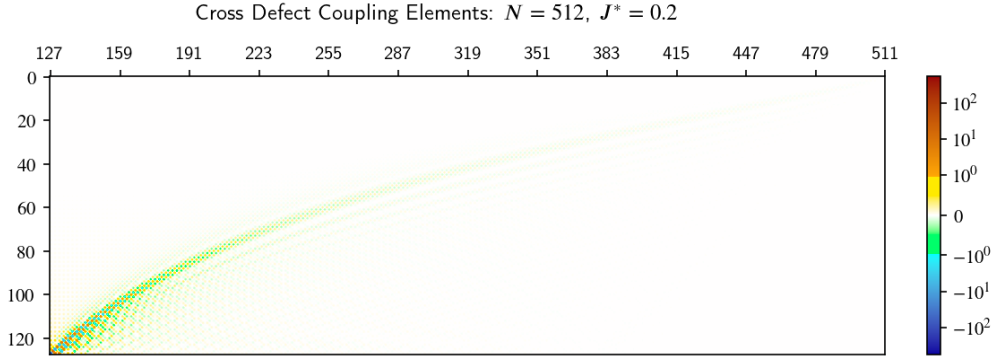


Figure 11: Zooming in on the cross defect coupling terms from figure 10c for $N = 512$.

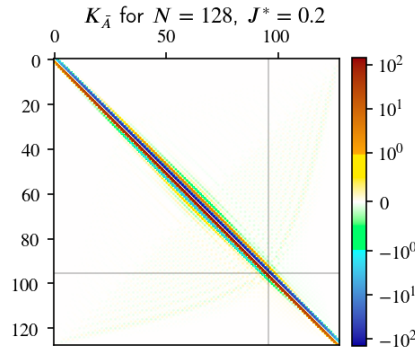


Figure 12: $K_{\bar{A}}$ for the off centered defect. The subsystem is the interval $[N/2, N - 1]$.

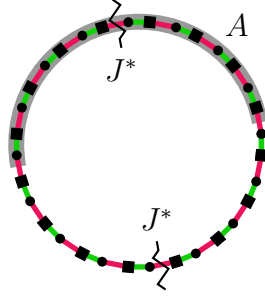


Figure 13: Diagram for the antipodal defects.

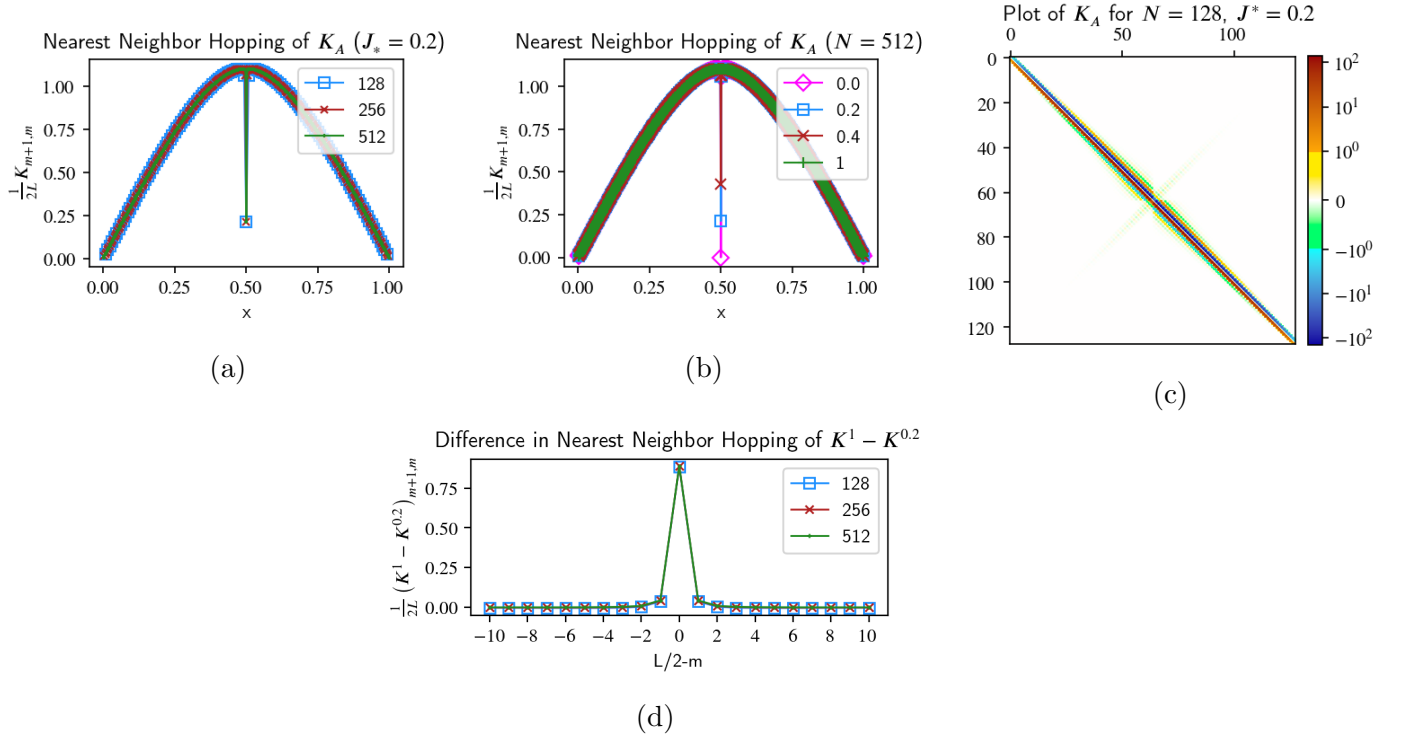


Figure 14: a) Plot of nearest neighbor interactions for various system sizes for $J^* = 0.2$. b) Plot of nearest neighbor interactions for various defects for $N = 512$. c) The full coupling matrix K for $N = 128$ and $J^* = 0.2$. Note that unlike the single defect case, the symmetric hopping terms are much less present. d) A plot of the nearest neighbor interactions for $K^1 - K^{0.2}$, where K^1 is the K matrix for no defect. The x axis is the lattice distance from the defect ($m = 0$). Like the single defect, the impact of the defect on the nearest neighbor hoppings is highly local.

4. Periodic with Antipodal Defects

In this section, we take a look at the case when there are two antipodal defects, as shown in figure 13. Like the case of the single defect, the nearest neighbor hoppings are only locally affected by the presence of the defect (figure 14abd). The nearest neighbor hopping terms (besides the defect bond itself) are less than 0.1% different from the

single defect, an agreement which gets better away from the defect and with increasing system size. However, the introduction of the antipodal defect in \bar{A} has the impact of decreasing the symmetric hopping terms seen in section 3 along with other cross defect couplings as seen in figure 15. This comes as no surprise, as when $J^* \rightarrow 0$, our system becomes two disconnect systems, with A containing two half system subsystems. Also, in a similar manner to the single defect, the strength of the symmetric hopping terms in terms of x is independent of N .

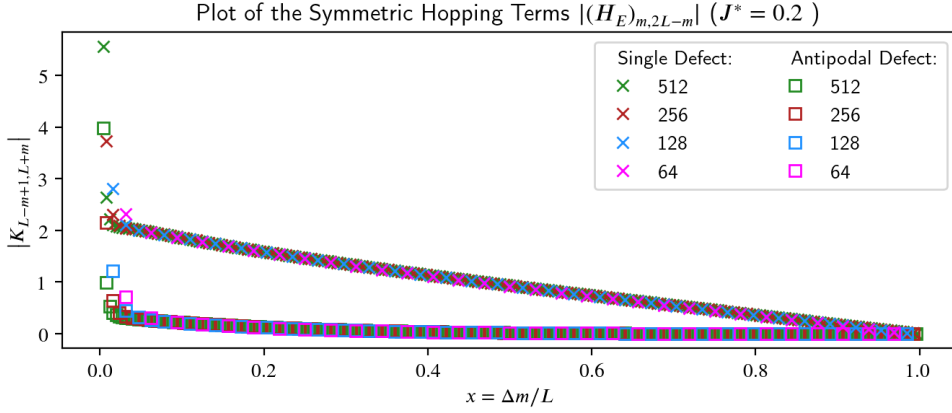


Figure 15: The symmetric hopping terms for both single and antipodal defects with $J^* = 0.2$.

5. Defects on Subsystem Boundary

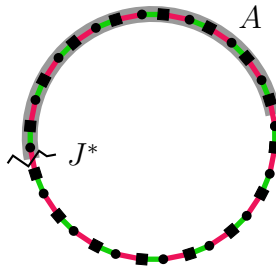


Figure 16: Diagram for the boundary defects.

5.1. One End

We begin with the usual $J^* = 0.2$ defect, now with the geometry shown in figure 16, which gives us the entanglement Hamiltonian in figure 17. On the edge with the defect, K_A is full of $\mathcal{O}(1)$ couplings, while the nearest neighbor couplings are relatively unchanged. This is not unexpected, as this is the end result of moving the defect towards the boundary, as was done in 3.2.

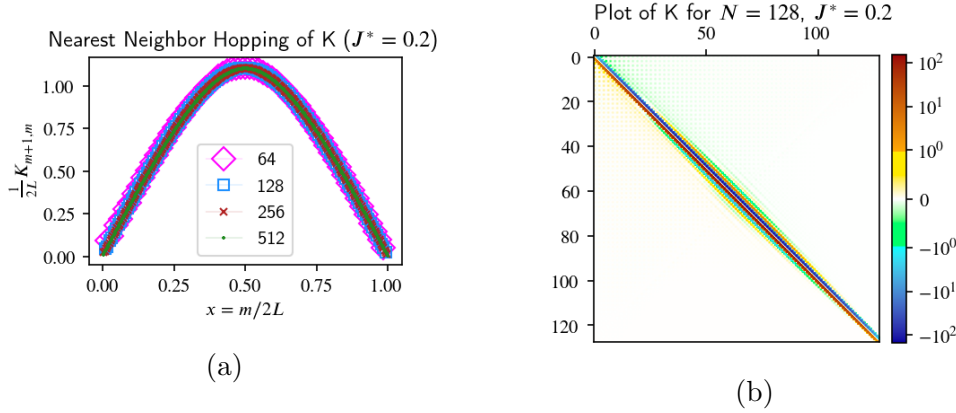


Figure 17: a) Plot of nearest neighbor couplings for the defect on the subsystem boundary. Note that the effect on the nearest neighbor hoppings is minimal. b) Plot of K for $J^* = 0.2$ as a comparison. Unlike previous K s, this matrix is highly non-local around the boundary with the defect.

Now that the defect is on the boundary, the natural question is how small do we need to make J^* to come to an entanglement Hamiltonian that resembles the one for the open system. This is the focus of figure 18. In 18abcd, we see K_A for decending bond strengths with $J^* = 0$ shown in d. Even for these very small couplings, the entanglement Hamiltonians contain large amounts of $\mathcal{O}(1)$ couplings. We also note that the nearest neighbor couplings at a fixed defect strength have a large dependence on system size (figure 18e). This behavior also translates over to the non-local terms; increasing N for a very small J^* increases the amount of non-local terms. This means that for larger system sizes, smaller couplings are needed to get close to the entanglement Hamiltonian of the open system in terms of the couplings present in K_A . However, using [12, 13], we calculate the infidelity between the open case and defects for $J^* = 10^{-5}$ and see that it is consistently $\mathcal{O}(10^{-12})$ as apposed to $\mathcal{O}(10^{-3})$ for $J^* = 0.2$ with $N = 64$. While the K_A matrices differ in their couplings, the states themselves are very close. §

This geometry was studied numerically in [14, 15] and analytically in [16, 17], where it is discussed that the entanglement entropy in this system goes as

$$S(L) = \frac{c_{\text{eff}} + c}{3} \log \left(\frac{N}{\pi} \sin \left(\frac{\pi L}{N} \right) \right) + S_0, \quad (5.1.2)$$

where L is the subsystem size and S_0 is a non-universal constant. c_{eff} is the effective

§ The fidelity is given by

$$F(\rho_{G_1}, \rho_{G_2}) = \left[\det \left(\frac{1 - G_1}{2} \right) \det \left(\frac{1 - G_2}{2} \right) \right]^{1/4} \left[\det \left(1 + \sqrt{\frac{1 + G_1}{1 - G_1}} \frac{1 + G_2}{1 - G_2} \sqrt{\frac{1 + G_1}{1 - G_1}} \right) \right]^{1/2}, \quad (5.1.1)$$

where the G_i s are the restricted correlation matrices.

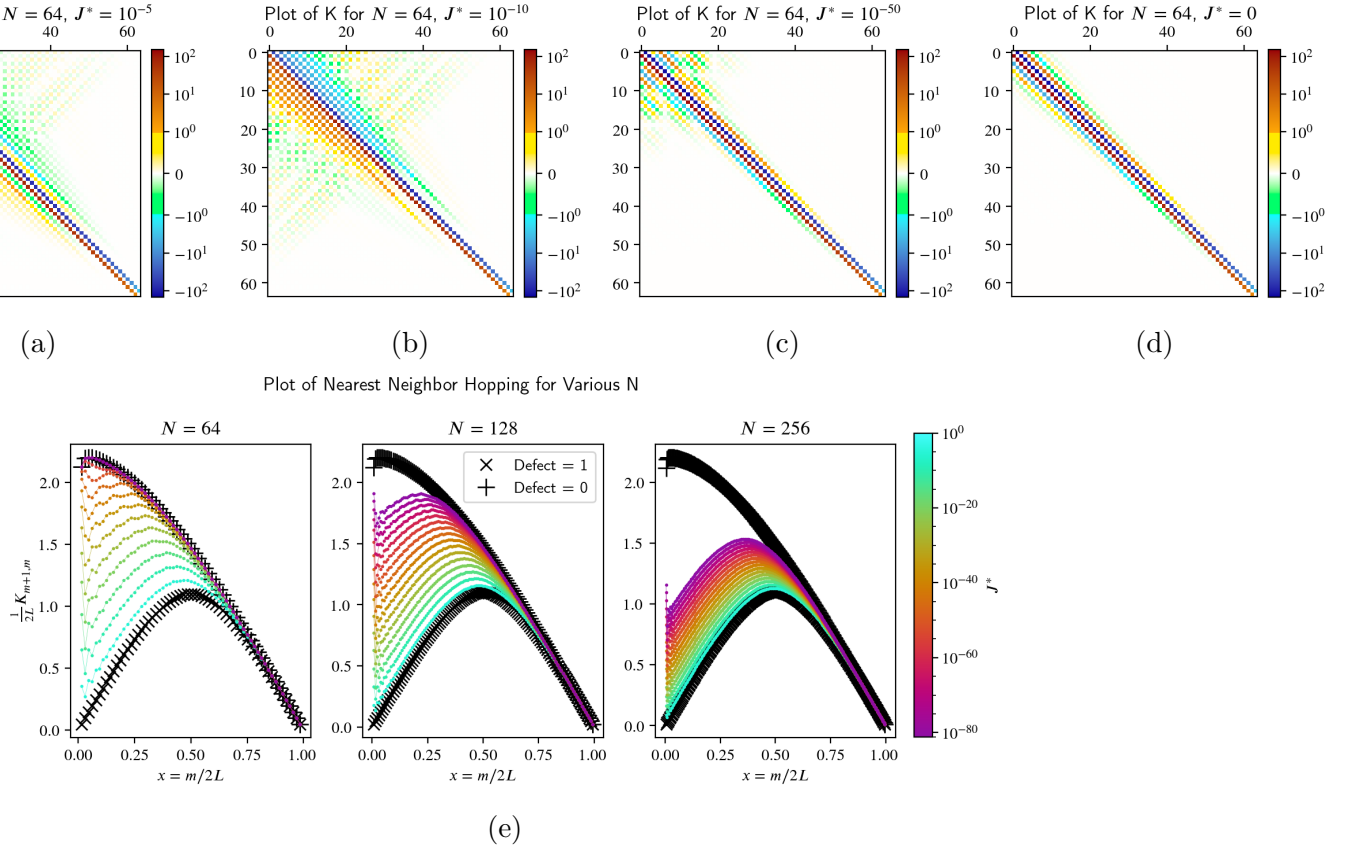


Figure 18: abcd) Plots of K for various small defects, with $J^* = 0$ corresponding to a open system where A is one half of the system. e) Plots of nearest neighbor interactions for various system sizes and defect strengths. Note that for larger system sizes, the same coupling strength moves farther away from the open system.

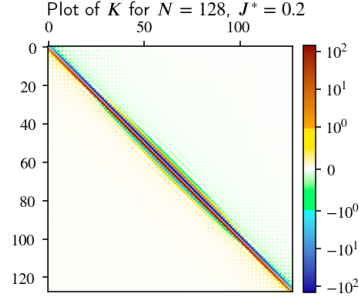
central charge defect on the boundary and is given by

$$c_{\text{eff}}(s) = \frac{s}{3} - \frac{1}{3} - \frac{3}{\pi^2} [(s+1) \log(s+1) \log(s) + (s-1) \text{Li}_2(1-s) + (s+1) \text{Li}_2(-s)] \quad (5.1.3)$$

where $s = |\sin[2(\cot^{-1}(J^*))]|$, and Li_2 is the dilogarithm function. For $J^* = 1$, $c_{\text{eff}} = c = 0.5$, which gives the standard $S(L) = \frac{1}{3} \log(\dots)$ for the critical Ising model. We will touch on this more in the conclusion; however, a next step that is beyond the scope of this paper is to find out how this behavior is represented in K_A .

5.2. Both Ends

To wrap up the boundary defects, we place a defect on both boundaries of A . For our standard $J^* = 0.2$, K_A (given in figure 19) has similar non-local terms as the single boundary defect, but now at both ends. We also know that for $J^* = 0$, A will be disconnected and K_A becomes undefined; however, we can probe small J^* to see what happens. We see that (figure 20) as $J^* \rightarrow 0$, all the couplings in K_A begin to grow.


 Figure 19: Plot of K with defects on the both edges of A .

In the same manor as the single defect, this rate of growth depends on the size of the system. This growth of terms in K_A is expected as it will drive up the entanglement energies of the excited states, pushing ρ_A towards that of a pure state.

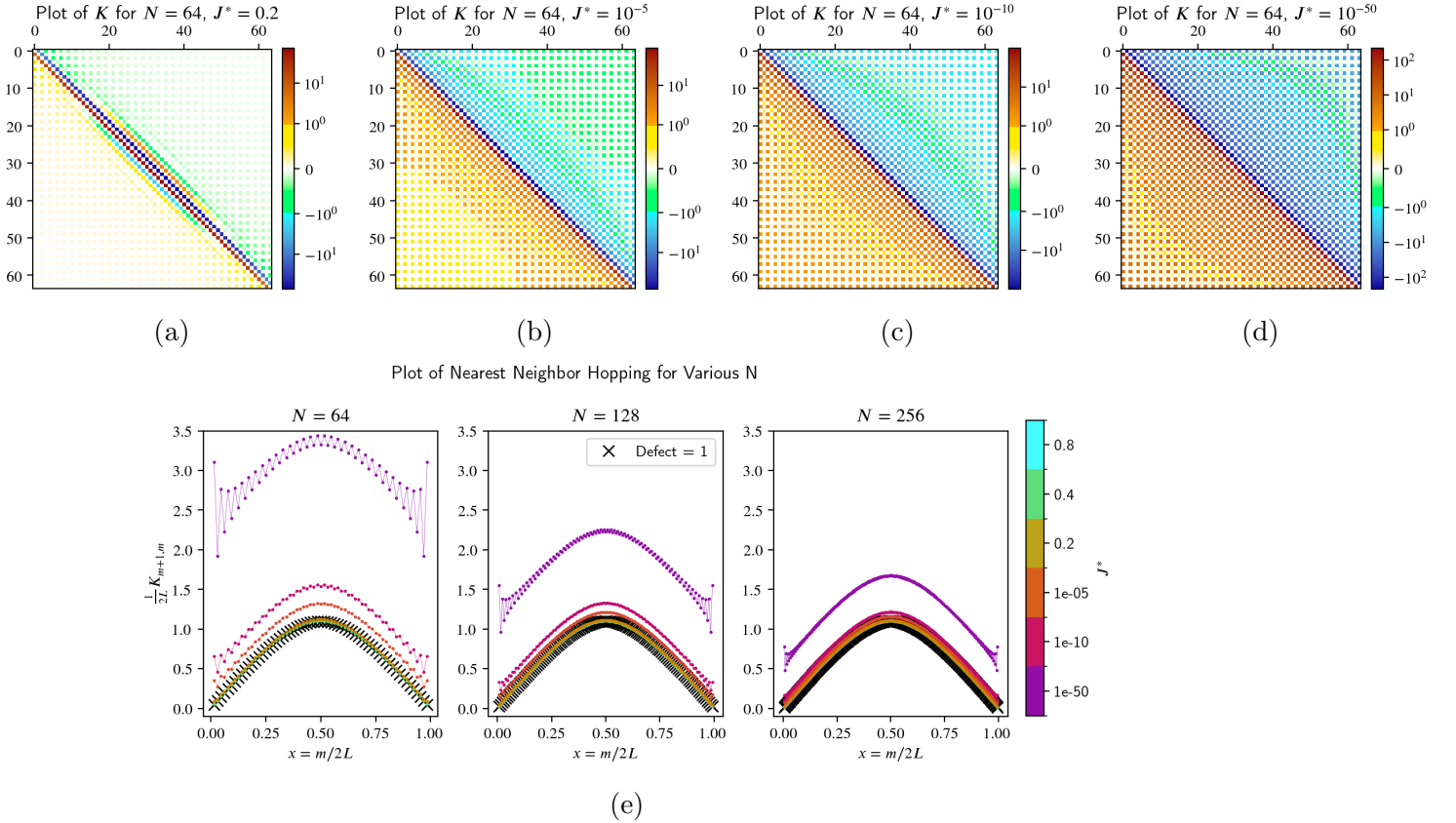


Figure 20: abcd) Plots of K for various small defects, with $J^* = 0$ corresponding to an open system where A is one half of the system. e) Plots of nearest neighbor interactions for various system sizes and defect strengths. Note that for larger system sizes, the same coupling strength moves farther away from the open system.



Figure 21: Diagram for the topological defects.

6. Defects With Zero Modes

We finish by looking at topological defects, which generate zero modes with the geometries shown in figure 21. For discussions on their effects on the entanglement entropy, see [18, 19], and for a CFT discussion on entanglement Hamiltonians for chiral zero modes, see [20].

6.1. Antiperiodic Defect

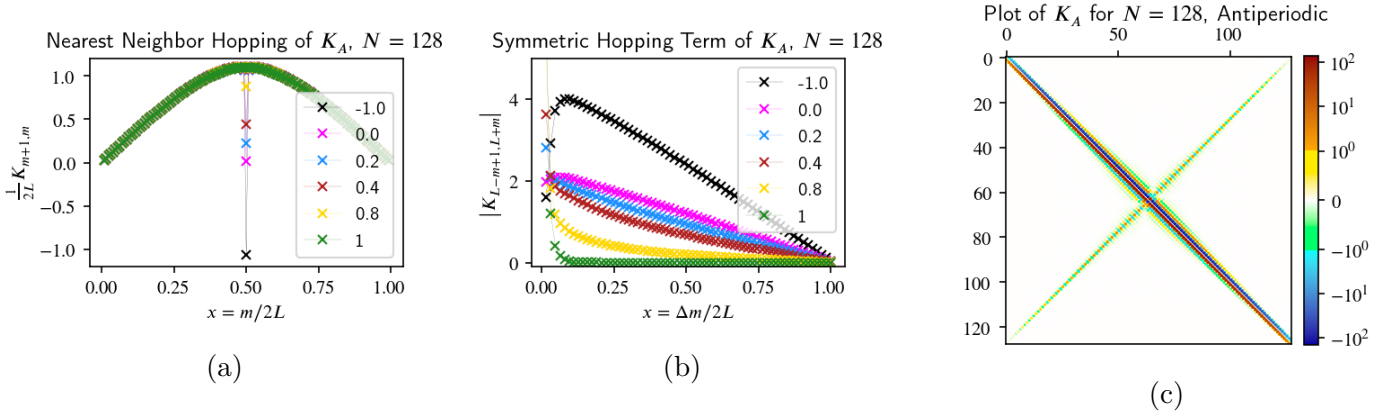


Figure 22: a, b) Plots of the nearest neighbor hopping and symmetric hopping terms for the centered defect, now containing the antiperiodic, $J^* = -1$ case. c) Plot of K_A for the antiperiodic system with defect centered in A .

Our last energy defect will be the case when $J^* = -1$. This is a topological defect that introduces a zero mode. In many ways, K_A behaves similarly to the case where we had a single centered energy defect from section 3. This can be seen in figure 22, where we see that the nearest neighbor hopping terms follow the same local rescaling for the defect site, and the plot of K has all the same features and not any more. In figure 22b, we also see that the symmetric hopping terms follow a similar pattern to the positive energy defects. In fact, if one were to add a few negative defects between 0 and -1 , one would see a smooth transition in these terms all the way from 1 to -1 .

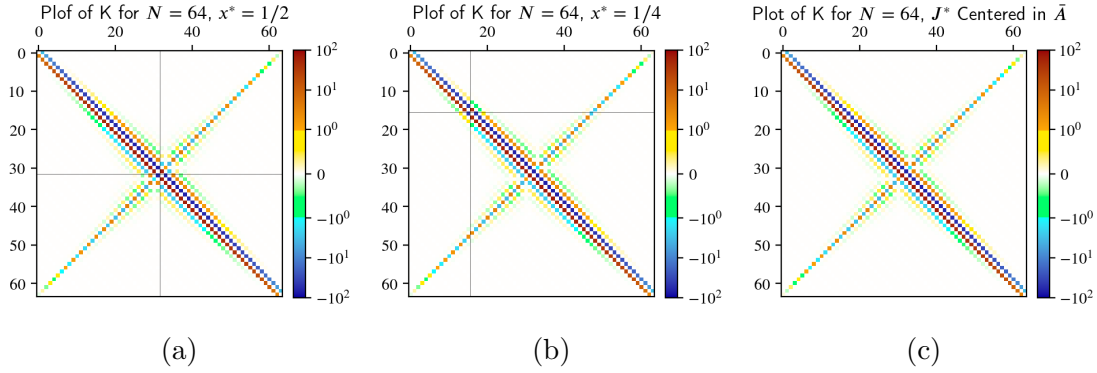


Figure 23: Plots of antiperiodic systems for different defect locations: Centered in A (a), Off centered in A (b) and centered in \bar{A} (c). Note that for when the defect is in A , all the bonds across the defect pick up a relative minus sign compared to when the defect is outside the subsystem. It is also worth noting that, while for c the defect is centered in \bar{A} , K is the same regardless of where the defect is, as long as it not a bond within A . The symmetric hopping term (up to a the possible aforementioned minus sign), is the same.

Because this is the topological defect, we also expect the K to be agnostic to the position of the defect. This is indeed the case if the defect is outside A ; however, if the defect is within A , then all cross defect couplings pick up a minus sign. This is seen in figure 23. Also, see in this figure is that the symmetric hopping terms are present and the same regardless of the defects location (up to the mentioned possible minus sign if the defect is in A); this is the manifestation of the translation invariance of the topological defect.

6.2. Duality Defect

We finally step away from the energy defect and now introduce a duality defect. In the Majorana language, this means skipping a single Majorana site in the chain. We again look at centered defects. As seen in figure 24a, the nearest neighbor couplings follow the standard arch, with two exceptions. These are the nearest neighbor Majorana hopping terms that are set to zero in the duality defect. Looking at figure 24c, we see that there is a gap in the nearest neighbor bonds, and in their place is an off centered bond which is the duality defect coupling. The vertical/horizontal elements are couplings to the skipped Majorana site generated by the zero mode. The couplings decay with system size (figure 24b). This is unlike the single defect symmetric hopping terms, which are system size independent.

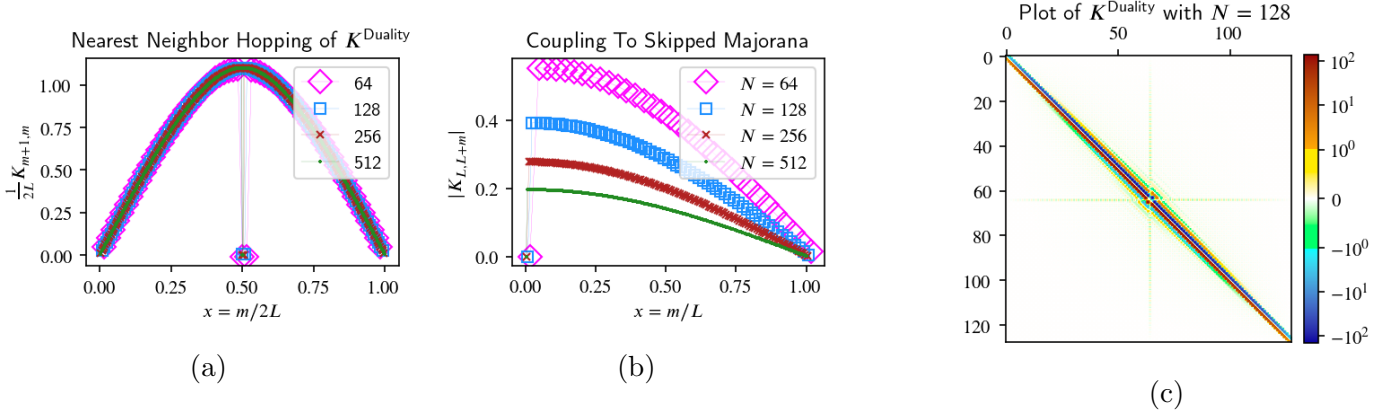


Figure 24: a) Nearest neighbor hopping terms of K . b) The couplings to the Majorana site that is skipped by the duality defect. These are the strongest non-local couplings in the system. Not that unlike the extra couplings in the antiperiodic system, these couplings become smaller as system size increases.

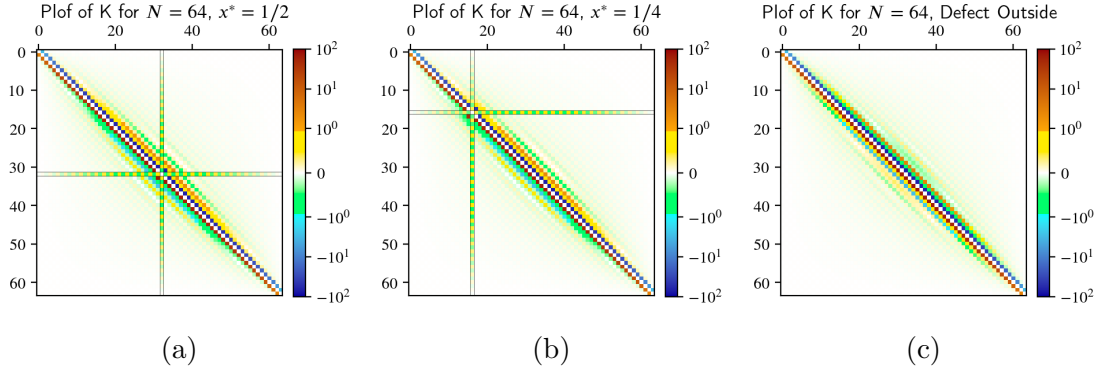


Figure 25: Plots of duality defect systems for different defect locations: Centered in A (a), Off centered in A (b) and outside of A (c). Like the antiperiodic defect, the location of the defect outside of A does not change K_A .

7. Conclusion and Future Work

We have seen that the introduction of defects, both topological and not, lead to non-local couplings in the entanglement Hamiltonian. Some of these non-local terms follow behaviors found in different configurations, such as the symmetric hopping term for the single energy defect and the bi-local component of the bipartite entanglement Hamiltonian for the CFT both being system size independent [3]. We have also seen non-trivial behavior for when boundary coupling is cut, where increasingly smaller bound strengths are required in order to get a K matrix that is similar in structure to the case where A is on one half of an open chain (even though the fidelity between the two states is very high). One of the next steps would be to calculate \mathcal{K} using CFT methods. This was done for defects in [21]; however, the system is an infinite line, which leads to the entanglement Hamiltonian for a defect centered in A being only local. For the periodic

system this should not be the case, as the lattice exhibits system size independent long range couplings and because the negativity across the defect is non-zero when the defect is purely reflective ($J^* = 0$). These properties are both tied to effective communication across the defect arising from communication through \bar{A} .

In [1, 2], it is discussed that the lattice entanglement Hamiltonian for no defects can be directly related to the local CFT result by taking a power series of $T \propto K_{\text{CFT}}$ where $[K_{\text{lattice}}, T] = 0$. Besides taking the CFT approach, one could use some kind of Hamiltonian fitting, such as the method described in [22], to try and find approximate entanglement Hamiltonians built out of only local and bi-local terms. As discussed in that paper, the method can reproduce the entanglement Hamiltonian for systems without defects, and the results it gets are precisely the expected CFT results. Using this technique to explore the nature of the long range couplings, especially which ones are needed, could be insightful to a CFT solution. It could also be useful in seeing how the effective central charge behavior of the entanglement entropy discussed in section 5.1 manifests itself in how the couplings are fit (and again, which couplings are required to get a good fit), along with providing insight into the relationship between the non-local couplings when looking at K_A and $K_{\bar{A}}$ for the single defect.

Acknowledgments

The author would like to thank Ananda Roy and David Rogerson for great discussions.

Bibliography

- [1] Eisler V and Peschel I 2017 *Journal of Physics A Mathematical General* **50** 284003 (Preprint [1703.08126](https://arxiv.org/abs/1703.08126))
- [2] Eisler V and Peschel I 2018 *Journal of Statistical Mechanics: Theory and Experiment* **2018** 104001 URL <https://dx.doi.org/10.1088/1742-5468/aace2b>
- [3] Eisler V, Tonni E and Peschel I 2022 *Journal of Statistical Mechanics: Theory and Experiment* **2022** 083101 URL <https://dx.doi.org/10.1088/1742-5468/ac8151>
- [4] Eisler V, Giulio G D, Tonni E and Peschel I 2020 *Journal of Statistical Mechanics: Theory and Experiment* **2020** 103102 URL <https://dx.doi.org/10.1088/1742-5468/abb4da>
- [5] Giulio G D, Arias R and Tonni E 2019 *Journal of Statistical Mechanics: Theory and Experiment* **2019** 123103 URL <https://dx.doi.org/10.1088/1742-5468/ab4e8f>
- [6] Dalmonte M, Eisler V, Falconi M and Vermersch B 2022 *Annalen der Physik* **534** 2200064 (Preprint <https://onlinelibrary.wiley.com/doi/pdf/10.1002/andp.202200064>) URL <https://onlinelibrary.wiley.com/doi/abs/10.1002/andp.202200064>

- [7] Peschel I 2003 *Journal of Physics A: Mathematical and General* **36** L205 URL <https://dx.doi.org/10.1088/0305-4470/36/14/101>
- [8] Latorre J I, Rico E and Vidal G 2004 *Quant. Inf. Comput.* **4** 48–92 (*Preprint quant-ph/0304098*)
- [9] mpmath development team T 2023 *mpmath: a Python library for arbitrary-precision floating-point arithmetic (version 1.3.0)* <http://mpmath.org/>
- [10] Shapourian H, Shiozaki K and Ryu S 2017 *Phys. Rev. B* **95**(16) 165101 URL <https://link.aps.org/doi/10.1103/PhysRevB.95.165101>
- [11] Shapourian H and Ryu S 2019 *Phys. Rev. A* **99**(2) 022310 URL <https://link.aps.org/doi/10.1103/PhysRevA.99.022310>
- [12] Banchi L, Giorda P and Zanardi P 2014 *Phys. Rev. E* **89**(2) 022102 URL <https://link.aps.org/doi/10.1103/PhysRevE.89.022102>
- [13] Zhang J and Rajabpour M A 2023 *Phys. Rev. A* **108**(2) 022414 URL <https://link.aps.org/doi/10.1103/PhysRevA.108.022414>
- [14] Roy A and Saleur H 2022 *Entanglement Entropy in Critical Quantum Spin Chains with Boundaries and Defects* (Cham: Springer International Publishing) pp 41–60 ISBN 978-3-031-03998-0 URL https://doi.org/10.1007/978-3-031-03998-0_3
- [15] Rogerson D, Pollmann F and Roy A 2022 *Journal of High Energy Physics* **2022** 165 (*Preprint 2204.03601*)
- [16] Brehm E M and Brunner I 2015 *JHEP* **09** 080 comments: 25 pages, 1 figure (*Preprint 1505.02647*) URL [https://link.springer.com/article/10.1007/JHEP09\(2015\)080](https://link.springer.com/article/10.1007/JHEP09(2015)080)
- [17] Peschel I and Eisler V 2012 *Journal of Physics A: Mathematical and Theoretical* **45** 155301 URL <https://dx.doi.org/10.1088/1751-8113/45/15/155301>
- [18] Roy A and Saleur H 2022 *Phys. Rev. Lett.* **128**(9) 090603 URL <https://link.aps.org/doi/10.1103/PhysRevLett.128.090603>
- [19] Capizzi L and Eisler V 2023 *Journal of Statistical Mechanics: Theory and Experiment* **2023** 053109 URL <https://dx.doi.org/10.1088/1742-5468/acd68f>
- [20] Klich I, Vaman D and Wong G 2017 *Phys. Rev. Lett.* **119**(12) 120401 URL <https://link.aps.org/doi/10.1103/PhysRevLett.119.120401>
- [21] Mintchev M and Tonni E 2021 *Journal of High Energy Physics* **2021** 205 (*Preprint 2012.01366*)
- [22] Zhu W, Huang Z and He Y C 2019 *Phys. Rev. B* **99**(23) 235109 URL <https://link.aps.org/doi/10.1103/PhysRevB.99.235109>